Journal of Japan Association for Earthquake Engineering, Vol. 19, No. 3, 2019

ATTENUATION CHARACTERISTICS OF MAJOR ACTIVE FAULTS ESTIMATED FROM TWOFOLD SPECTRAL RATIO METHOD

Masayuki YAMADA[1] and Yoshiya ODA[2]

[1] Non-member of JAEE, Manager, Newjec Inc., Osaka, Japan
yamadams@newjec.co.jp
[2] Member of JAEE, Associate Professor, Department of Civil and Environmental Engineering, Tokyo Metropolitan University, Tokyo, Japan, oda@tmu.ac.jp

ABSTRACT: This study presents the relation between the estimated P-wave attenuation characteristics across the active fault line and the stress state characteristics of the fault for the 12 major active faults in Japan. We employed a twofold spectral ratio method to estimate the attenuation characteristics of the active faults. As a result of a review of the differences in the attenuation characteristics, a clear positive correlation with the ratio of the lapse time from the previous earthquake was confirmed. These results suggest that the attenuation characteristics estimated in this study may reflect the stress state of the active fault.

Key Words: twofold spectral ratio method, major active fault, attenuation characteristics, stress accumulation process

1. INTRODUCTION

Recently, information on active faults in Japan has been actively organized, analyzed, and publicly presented mainly by the national institutions. Among such institutions, the Headquarters for Earthquake Research Promotion has selected “Major Active Faults” by considering the seismicity, extent of influence of seismic activity on society, etc., and evaluated, publicized, and prioritized such zones, thus aiming to contribute to the mitigation of damage by earthquakes. The long-term evaluation of the major active faults has appropriately compiled locations, patterns, and past activities as a highly important and helpful resource to be used for the mitigation of the damage by earthquakes. However, any reference to the active fault properties of stress or strain cannot be found in the presented evaluation document.

It is clear that identification of the stress state and strain accumulation process in active faults whose future movement is predicted can enhance the importance and usability of data in the mitigation of earthquake damage. As the first step to understand the state of the stresses and strains in the active faults, researchers have conducted studies to identify the physical properties and their variations in the seismic source area. For example, Poupinet et al.[1)] confirmed the precise travel-time variations of seismic waves in the focal region of the Coyote Lake Earthquake (M5.9) in 1979 and noted that the S-wave velocity decreased by 0.2% in the focal region after the main shock than before. Uchida et al.[2)]

conducted artificial seismic experiments in the focal region of the 1998 Northern Iwate Prefecture Earthquake (M6.1) and detected a reduction in velocity of from 0.1% to 0.9% after the main shock than before. The authors mentioned that this variation can be explained by stress variations due to the occurrence of an earthquake; however, they also noted that the variations in seismic wave velocity occurred not in the limited range near the fault but in a relatively wide range. As in these studies, it has been confirmed that the seismic wave velocity after the occurrence of an earthquake in a focal region tends to lower, though the variation is extremely minor. Although these studies suggest the possibility of extracting fault characteristics variation according to seismic wave velocity, it seems that there is a limitation to detecting the variation of characteristics of the thin active fault itself.

On the other hand, as the characteristics and stress states of focal regions can be estimated according to attenuation characteristics, studies are not negligible to extract attenuation characteristics for the focal regions. Nakamura et al.[3] researched attenuation along the Rokko Fault after the 1995 Southern Hyogo Prefecture Earthquake and noted the existence of a high Q_s^{-1} (low Q_s) value which they interpreted as disturbance and internal attenuation due to inhomogeneous properties in the fault zone. Lees and Lindley [4] estimated three-dimensional attenuation tomography in the focal region of the 1989 Loma Prieta Earthquake and presented the existence of high Q_p and low Q_s ranges surrounding the aftershock region. They concluded that this was because the pores in the fault zone were saturated with fluid. Chun et al.[5] discussed temporal changes in attenuation characteristics using long-term observation data also in source area of the Loma Prieta Earthquake. Blakeslee et al.[6] estimated the attenuation of the San Andreas Fault using a spectral ratio and noted the existence of a low Q_s. The authors of this study attempted to clarify temporal changes in the spectral ratio before and after the 2008 Iwate-Miyagi Nairiku Earthquake [7]. As all the existing studies focus on variations in attenuation characteristics after an earthquake or after an earthquake than before, the target faults and the available earthquake records are limited. In other words, it can be said that there are few studies that have comprehensively clarified the attenuation characteristics of active faults in a certain country or region.

Under these circumstances, this study used observation records from the High Sensitivity Seismograph Network of Japan (Hi-net), of the National Research Institute for Earth Science and Disaster Resilience (NIED) to cover the major active fault zones in Japan and estimated the P-wave attenuation characteristics for each active fault according to the seismic waves passing through them. We then examined the relationship between the already evaluated and publicized characteristics of the major active faults and the attenuation characteristics obtained in this study.

2. THE TWO FOLD SPECTRAL RATIO METHOD

In this study, attenuation characteristics of the active faults were estimated using the seismic waves passing through the faults. The twofold spectral ratio method was used for this purpose [8]. This method can be used to estimate the propagation path characteristics (attenuation characteristics) by removing the source characteristics and site-amplification characteristics from the multiple seismic records of multiple observation points [9), 10), 11)]. Although the attenuation characteristics normally obtained using the twofold spectral ratio method is an average of the entire ray path, in this study, we estimated the attenuation characteristics of certain regions (active faults) by improving the selection of the source and observation points. As shown in Figure 1, we examined two observation points across the active fault and the two earthquakes (Earthquake 1 and Earthquake 2) which occurred on both sides of the extensions.

In this case, the amplitude spectrum of the observation record for the observation point A in Earthquake 1, $O_{1A}(f)$, can be expressed as is shown in equation (1) using source spectrum, $S_1(f)$, propagation-path characteristics, $P_{1A}(f)$, and site-amplification characteristics, $G_A(f)$ [12)]:

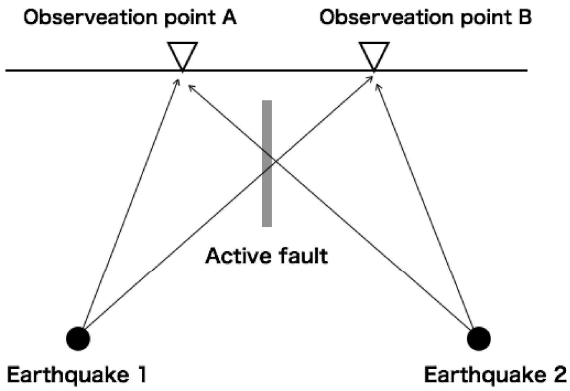

Fig. 1 Arrangement of the active fault, observation points and earthquakes used for the twofold spectral ratio method

$$O_{1A}(f) = S_1(f) \cdot P_{1A}(f) \cdot G_A(f) \tag{1}$$

The Fourier amplitude spectral ratio, which refers to the amplitude of an observation point (observation point B in this case) passing through the fault to that of an observation point (observation point A in this case) not passing through the fault in the record of Earthquake 1, is expressed using equation (2) wherein the source characteristics are eliminated:

$$\frac{O_{1B}(f)}{O_{1A}(f)} = \frac{S_1(f) \cdot P_{1B}(f) \cdot G_B(f)}{S_1(f) \cdot P_{1A}(f) \cdot G_A(f)} = \frac{P_{1B}(f) \cdot G_B(f)}{P_{1A}(f) \cdot G_A(f)} \tag{2}$$

In the same manner, the spectral ratio for Earthquake 2 is expressed using equation (3) as follows:

$$\frac{O_{2A}(f)}{O_{2B}(f)} = \frac{S_2(f) \cdot P_{2A}(f) \cdot G_A(f)}{S_2(f) \cdot P_{2B}(f) \cdot G_B(f)} = \frac{P_{2A}(f) \cdot G_A(f)}{P_{2B}(f) \cdot G_B(f)} \tag{3}$$

Furthermore, multiplying these spectral ratios (twofold spectral ratio), the site-amplification characteristics of observation points A and B are eliminated and equation (4) is provided as follows:

$$\frac{O_{1B}(f)}{O_{1A}(f)} \cdot \frac{O_{2A}(f)}{O_{2B}(f)} = \frac{P_{1B}(f)}{P_{1A}(f)} \cdot \frac{P_{2A}(f)}{P_{2B}(f)} \tag{4}$$

If Earthquakes 1 and 2 are sufficiently distant compared to the intervening distance between the observation points, it can be considered that the ray paths to the vicinity of the observation points are almost identical. Accordingly, it is expected that the right side of the equation (4) is equal to the square of the propagation path characteristics between the observation points. When setting the source distance to R_{ij}, the circumference ratio to π, the elastic-wave velocity to V, and the Q-value to Q, the propagation-path characteristics to earthquake i and observation point j, $P_{ij}(f)$, can be expressed as in equations (5) and (6) [13] as follows:

$$P_{ij}(f) = \frac{1}{R_{ij}} \exp(-\alpha_{ij}) \tag{5}$$

$$\alpha_{ij} = \frac{\pi f}{QV} R_{ij} \tag{6}$$

Substituting the equation (5) into the equation (4) and correcting the geometric attenuation according to the ratio of source distance to the twofold spectral ratio calculated from the observation records, the attenuation characteristics between the observation points A and B can be obtained as in equation (7) as follows:

$$\left(\frac{O_{1B}(f)}{O_{1A}(f)} \cdot \frac{O_{2A}(f)}{O_{2B}(f)} \cdot \frac{R_{1B}}{R_{1A}} \cdot \frac{R_{2A}}{R_{2B}} \right)^{\frac{1}{2}} = \exp\left(-\alpha_{AB}\right) \tag{7}$$

Furthermore, according to equation (6) and equation (7), the Q-value between the observation points can be determined as in equation (8) as follows:

$$Q = \frac{-2\pi R_{AB}}{V \cdot \ln \left(\frac{O_{1B}(f)}{O_{1A}(f)} \cdot \frac{O_{2A}(f)}{O_{2B}(f)} \cdot \frac{R_{1B}}{R_{1A}} \cdot \frac{R_{2A}}{R_{2B}} \right)} f \tag{8}$$

The right side of equation (7), α_{AB}, is calculated precisely using the difference in the source distance according to equations (4)–(6), namely (R_{1B} - R_{1A} + R_{2A} - R_{2B}) / 2. However, assuming that the ray path to the vicinity of the observation points becomes nearly the same when the source is sufficiently distant, the difference in the source distance is approximated using the distance between the observation points, R_{AB}, in equation (8). Applying the twofold spectral ratio method as described, the attenuation characteristics between the observation points are extracted.

3. SELECTION OF THE ACTIVE FAULTS TO BE EXAMINED FOR ATTENUATION CHARACTERISTICS

3.1 Extraction of examination target candidate active faults and observation points

Among the earthquakes for which the Headquarters for Earthquake Research Promotion (hereinafter referred to as the "Earthquake Headquarters") conducted long-term evaluation [14] and estimated fault parameters, active faults with the estimated moment magnitude of 7.0 or greater and with a pair of observation points across the fault within a distance of 40 km between the points were selected in this study as the examination target candidates. Although the setting of 40 km has no physical basis, the interval between the observation points for Hi-net is approximately 20 km and accordingly the interval in this study is set to within two times of this value. Under this condition, 21 active faults and pairs of observation points as shown in Table 1 were selected as examination target candidates.

3.2 Selection of earthquake data

Earthquake data was selected for the active faults and pairs of observation points selected as described in Section 3.1. For the extraction of attenuation characteristics of the active faults according to the twofold spectral ratio, it is necessary to remove the source and propagation path characteristics. Borcherdt [15] and Fujimoto and Midorikawa [16] used observation points with an interval, of less than 25 km and 30 km respectively as observation point pairs having source and propagation path characteristics in common. In this study, as the observation point interval was set to within 40 km for the selection of observation point pairs across the fault, a condition that an earthquake should be at a distance of five times or farther away as the observation point interval was added to ensure the

Table 1 Examination target candidate active faults and the observation point pairs

No.	Fault zone	OBS Point pair OBS1	OBS2	Point 1 Lat. (deg)	Long. (deg)	Point 2 Lat. (deg)	Long. (deg)	Distance (km)
1	Shibetsu fault zone	N.SYSH	N.STNH	43.9271	144.8075	43.7851	145.0246	23.5
2	Tokachi low-land fault zone main part	N.MMRH	N.TYRH	42.8920	143.0603	42.8114	143.5203	38.7
3	Ishikari low-land Eastern margin fault zone main part	N.OIWH	N.YUBH	42.8739	141.8191	42.9930	142.0085	20.3
4	Oritsume fault zone	N.NHEH	N.KHEH	40.2383	141.3423	40.1533	141.4245	11.9
5	Kitakami low-land Western margin fault zone	N.HMSH	N.TOUH	39.3434	141.0473	39.3340	141.3015	21.9
6	Nagai Basin Western margin fault zone	N.ONIH	N.NYOH	37.9881	139.8016	38.1035	140.1552	33.6
7	Aizu Basin Eastern margin fault zone	N.ATDH	N.SMGH	37.4508	139.8126	37.2544	139.8725	22.8
8	Fukaya fault zone	N.ISSH	N.KWTH	36.3143	139.1847	36.1131	139.2894	24.1
9	Nagano Basin Western margin fault zone	N.MKOH	N.NZWH	36.9425	138.2594	36.9102	138.4408	16.3
10	Ouchigata fault zone	N.SHKH	N.HIMH	37.0533	136.8206	36.8866	136.9276	20.8
11	Sakaitoge-Kamiya fault zone	N.KSOH	N.TTNH	35.9632	137.7669	36.0087	137.9305	15.6
12	Inadani fault zone main part	N.AGMH	N.INHH	35.7870	137.7173	35.8315	137.9236	19.2
13	Shokawa fault zone	N.SYKH	N.TMAH	36.0654	136.9479	36.1337	137.2208	25.5
14	Atera fault zone main part	N.GR2H	N.HSKH	35.7991	137.2531	35.6401	137.3187	18.4
15	Yourou-Kuwana-Yokkaichi fault zone	N.KYSH	N.KGIH	35.2177	136.8509	35.3059	137.0570	21.2
16	Suzuka Eastern margin fault zone	N.KIDH	N.HMAH	35.2953	136.4732	35.2768	136.7002	20.7
17	Kyoto Nishiyama fault zone	N.SSYH	N.KMEH	35.0708	135.2811	35.0469	135.4846	18.8
18	Uemachi fault zone	N.KNHH	N.OSKH	34.6628	135.3896	34.7159	135.5199	13.3
19	Median Tectonic Line fault zone Sanuki Mountains southern margin-Ishizuchi Mountains northern margin east part	N.IKWH	N.AYKH	33.9997	133.8932	34.2186	133.9493	24.9
20	Iwakuni fault zone	N.MKWH	N.IKNH	34.1974	131.9943	34.1891	132.1260	12.3
21	Kikugawa fault zone	N.MNEH	N.KIKH	34.1149	131.0506	34.1111	131.1434	8.6

The gray-shaded part indicates a fault zone not covered by the analysis.

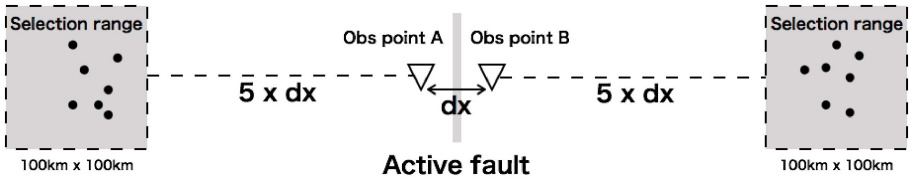

Fig. 2 Method for the setting of earthquake selection range

selection of sufficiently distant earthquakes. However, as discussed later, the maximum distance of the ultimate analysis target observation point pairs was 25.5 km, and therefore, it can be considered that it was equivalent to the selection of earthquake data under the same conditions as the studies of Borcherdt [15] and Fujimoto and Midorikawa [16].

During the first step of the selection of earthquakes, the distance which is five times the observation point distance (5 × dx), as shown in Figure 2, is set to the orthogonal direction of the target active fault trend. Next, a 100-km square range outside the points is established to analyze the earthquakes occurred within the range. To be precise, earthquakes of magnitude 2.0 or greater were selected from the Japan Meteorological Agency Unified Hypocenter Catalogues. Figure 2 shows the method for establishing the selection range. Although earthquakes are selected from both sides in an orthogonal direction to the active fault trending direction in an actual situation, it is noted as the east side and the west side based on the relative positional relation. For example, in the case of the Median Tectonic Line fault zone (trending direction: N70°E) nearest the east-west direction, an earthquake on the north side is noted as the west side and an earthquake on the south side is noted as the east side.

In the case that distant earthquakes are employed, it may be impossible to sufficiently remove the propagation path characteristics to the vicinity of the observation points and the site-amplification characteristics even after calculating the twofold spectral ratio because of a slight difference in wave-line path and other appropriate factors. In order to reduce these influences, an evaluation is conducted by determining the mean spectral ratio of multiple earthquakes. To decide the number of

earthquakes to employ in this study, we confirmed how the spectral ratios (mean value) of observation point pairs varied according to the number of earthquakes in the Oritsume fault zone where many earthquakes were observed. As the first step, 100 earthquakes were selected as previously described and used to determine the spectral ratios and the mean value. Then, spectral ratios were calculated by varying the number of earthquakes and the correlation coefficients to the spectral ratios calculated with the 100 earthquakes, respectively, in the fault-trending direction component and for the orthogonal-trending component. Figure 3 shows the relationship between the number of earthquakes and correlation coefficients. As the correlation coefficient exceeds 0.95 when the number of earthquakes is seven, a total of 14 earthquakes were used for analysis by selecting seven earthquakes, respectively, from both sides of all active faults. In the calculation of spectral ratios, the P-wave first motion part, whose wave-line path is relatively clear, was used. To be specific, the P-wave first motions in each earthquake record were read and the data for 5.12 seconds from 0.5 seconds before the P-wave first motions were used for analysis.

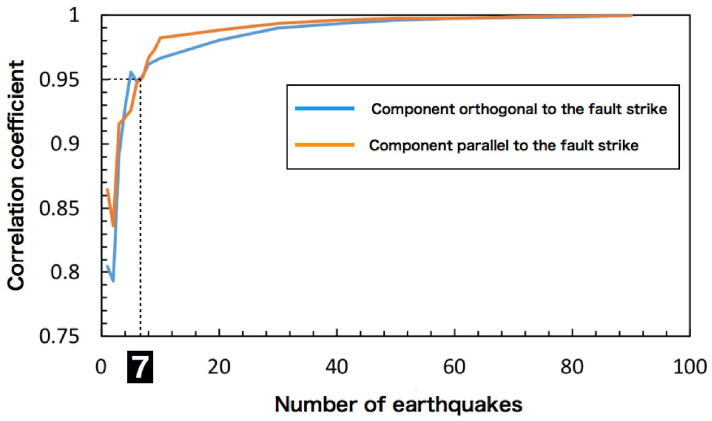

Fig. 3 Correlation with spectral ratios calculated using 100 earthquakes

3.3 Confirmation of ray path

To extract attenuation characteristics in the vicinity of active faults, wave lines need to pass through the target faults. Therefore, we confirmed the wave-line paths for the earthquakes selected as described in Section 3.2 by wave-line tracing. For wave-line tracing, we employed the Pseudo-Bending method [17] and created the velocity structure model referring to the JMA2001 [18] (Table 2). We calculated the detailed wave lines using SIMULPS [19].

We referred to the Long-Term Evaluation [14] of the Earthquake Headquarters for locations, trending directions and angles of inclination of active faults as a rule and also used data from the Japan Seismic Hazard Information Station (J-SHIS) [20] of the NIED as a supplementary reference regarding unclear items such as angles of inclination. Figure 4 shows the wave-line paths of the Oritsume fault zone and the Kitakami low-land fault zone. Figure 4 presents the wave-line paths in a cross section in the orthogonal direction to the trending direction of the active faults. As shown in the figure, it is highly likely that wave lines pass through the active faults in the Oritsume fault zone a shown in figure 4 a. In contrast, it is highly likely that wave lines do not pass through the active faults in the Kitakami low-land fault zone as shown figure 4 b. Accordingly, the Kitakami low-land fault zone was removed from examination in this study. We also removed active faults where more than 14 earthquakes were not obtained or where wave lines did not pass through, and as a result, we decided to examine the attenuation characteristics of 12 active faults after removing the gray-shaded faults of the active faults listed in Table 1. We provide wave-line paths of all the active faults as an Appendix to this study.

Table 2 Velocity structure used for ray tracing

Depth(km)	V_p(km/s)
0.0	4.80
1.0	5.09
2.0	5.34
3.0	5.55
4.0	5.72
5.0	5.82
6.0	5.86
7.0	5.90
8.0	5.94
9.0	5.98
10.0	6.02
11.0	6.06
12.0	6.10
13.0	6.14
14.0	6.18
15.0	6.22
16.0	6.26
17.0	6.31
18.0	6.35
19.0	6.40
20.0	6.45
150.0	8.11

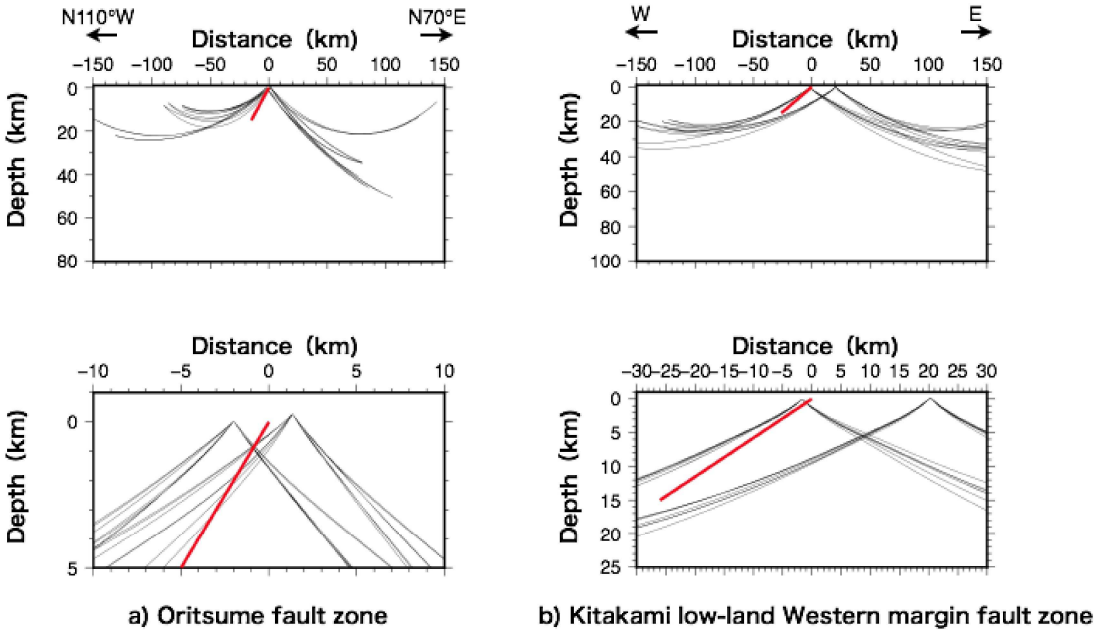

Fig. 4 Relationship between active faults and ray paths according to the ray tracing: a) Oritsume fault zone, b) Kitakami low-land western margin fault zone. A solid red line indicates an active fault. A thin solid line indicates a ray path. The lower figures show the enlarged figures of active fault parts.

4. DETERMINATION OF ATTENUATION CHARACTERISTICS ACCORDING TO THE TWOFOLD SPECTRAL RATIO METHOD

4.1 Determination of the spectral ratios of observation point pairs

As mentioned in Chapter 3, we conducted an analysis of 12 active faults by selecting 14 earthquakes occurring on both sides of the faults. As the first step, the P-wave first motions of corresponding earthquakes are read from the continuous observation records of Hi-net to cut out the data for 5.12 s from 0.5 s before. After correcting the installation directions by referring to the observatory station information in Hi-net, cos-shape tapering is then carried out to 10% of both the ends and Fourier amplitude spectra are calculated. After this step, smoothing is conducted with a Parzen window with a bandwidth of 0.8 Hz, and the spectral ratios of observation point pairs to the earthquakes occurring on both sides of the active faults are calculated as shown in equation (2) and equation (3). As P-wave first motions are used in this study, we analyzed the components that are orthogonal to the fault strike direction as radial components. Figure 5 shows the spectral ratios of observation point pairs calculated for the Oritsume fault zone. Figure 5a shows the spectral ratios calculated from the earthquakes on the east side of the active faults. Figure 5b shows the spectral ratios calculated from the earthquakes on the west side. The thin solid lines in the figures indicate spectral ratios of individual earthquakes and the thick line indicates the mean values. Although a slight unevenness is identified for the earthquakes, nearly stable spectral ratios are obtained. During this stage, as the site-amplification characteristics have not been eliminated, a difference is identified in the spectral ratios on both sides. We provide all spectral ratios as an Appendix to this study.

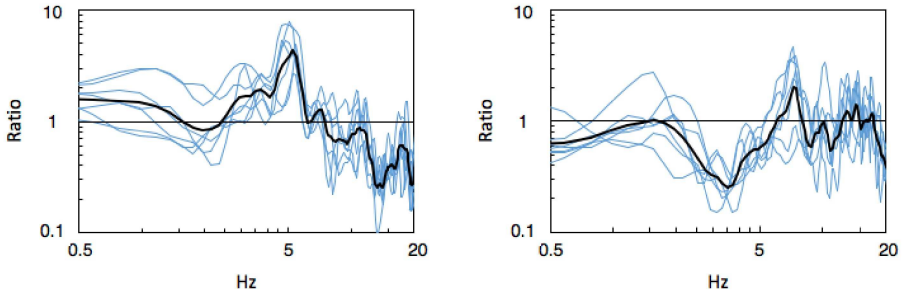

a) Spectral ratios for earthquakes on the east side b) Spectral ratios for earthquakes on the west side

Fig. 5 Spectral ratios for earthquakes on both sides of active faults (e.g., the Oritsume fault zone)

4.2 Results of the determination of attenuation characteristics

Using the spectral ratios of observation point pairs, the twofold spectral ratio is calculated as shown in equation (7). As in equation (6), the twofold spectral ratio is a function of observation point intervals. To compare the extent of attenuation in each active fault, distance correction is performed to the mean observation point interval (18.4 km) of the Atera fault zone. Although it is necessary to perform distance correction based on the ray path distance to be precise, correction in this study is performed for the straight-line distance between observation points. Figure 6 shows the twofold spectral ratios for 12 active faults. The dotted line in the figures indicates the mean value of twofold spectral ratios between 0.5 Hz and 20 Hz (hereinafter referred to as the mean twofold spectral ratio). As a result of the analysis, the mean twofold spectral ratio of the Oritsume, Nagano Basin Western margin, Inadani, Atera, Suzuka Basin Eastern margin, and Uemachi fault zones is 0.76, 0.50, 0.63, 0.77, 0.83, and 0.60, respectively, indicating an attenuation tendency. On the other hand, the mean twofold spectral ratio of the Aizu Basin Eastern margin, Fukaya, Sakaitoge-Kamiya, Shokawa, Median Tectonic Line (Sanuki Mountains south margin and Ishizuchi Mountains Northern margin East region), and Iwakuni fault zones is 1.08, 0.91, 1.28, 0.93, 0.90, and 1.33 respectively, indicating a nearly flat or have a slight

amplification tendency. As the values for the Oritsume fault zone are small between 0.8 Hz and 4 Hz and large between 4 Hz and 8 Hz, the fluctuation in spectral ratio is more prominent than that of the other faults.

As is shown in the ray paths, it is difficult to examine the difference in attenuation characteristics according to the difference in depth because ray paths do not always pass through active faults at the same depth. We consider that the attenuation characteristics obtained in this study show the mean characteristics of active faults.

5. DISCUSSION

5.1 Examination of the unevenness in spectral ratios

As mentioned in Chapter 4, as a result of the determination of twofold spectral ratios of 12 active faults, we confirmed that the extent of attenuation differs depending on the active fault. In this study, we extracted the attenuation characteristics of active faults under the assumption that source and propagation-path characteristics can be removed by calculating the spectral ratios of sufficiently distant earthquakes. If this assumption is valid, it is expected that all the spectral ratios of the seven earthquakes on one side of each active fault reflect the attenuation characteristics and the site-amplification characteristics between the observation points and that the ratios are similar. Accordingly, we calculated the common logarithm standard deviation of each frequency of spectral ratios in the seven earthquakes on one side of each active fault and determined the mean value (Table 3). According to the calculation result, the standard deviation of the Fukaya, Atera and Suzuka eastern margin fault zones is 0.25 or greater; however, the standard deviation of the other active faults is approximately equal to 0.2 or is less, which is not a high value.

5.2 Cases where the spectral ratio exceeds 1

As described in Section 4.2, the results show that the mean twofold spectral ratio of the Aizu Basin eastern margin fault zone and the Sakaitoge-Kamiya fault zone exceeds 1. In order to examine the result, the spatial location relationship among ray paths connecting to the observation points and sources, the surrounding active faults [20], and volcanoes [21] is shown in figure 7.

In the Aizu Basin eastern margin fault zone, as the Aizu Basin western fault zone and the Numazawa Volcano exist near the observation point (N.ATDH) on the west side, it is possible that seismic waves from the west side which do not cross the fault are affected by them. This may cause a greater attenuation than that in the observation point (N.SMGH) on the east side which crosses the fault.

In the Sakaitoge-Kamiya fault zone, active faults and a volcano also exist in the surrounding area, and furthermore, conjugated active faults such as the Mutouyama-Narai fault zone exist between the observation points. In this way, an extremely complex underground structure can have a significant influence on the value of the twofold spectral ratio.

In the Iwakuni fault zone, the observation point (N.IKNH) on the east side is nearly directly above the fault. According to the evaluation by Earthquake Headquarters that the inclination of the fault is high-angled to the northwestern side, it is predicted that the location deep under the ground is slightly closer to the northwestern side than the location described in the figure; however, the wave lines may not pass through the active fault as expected.

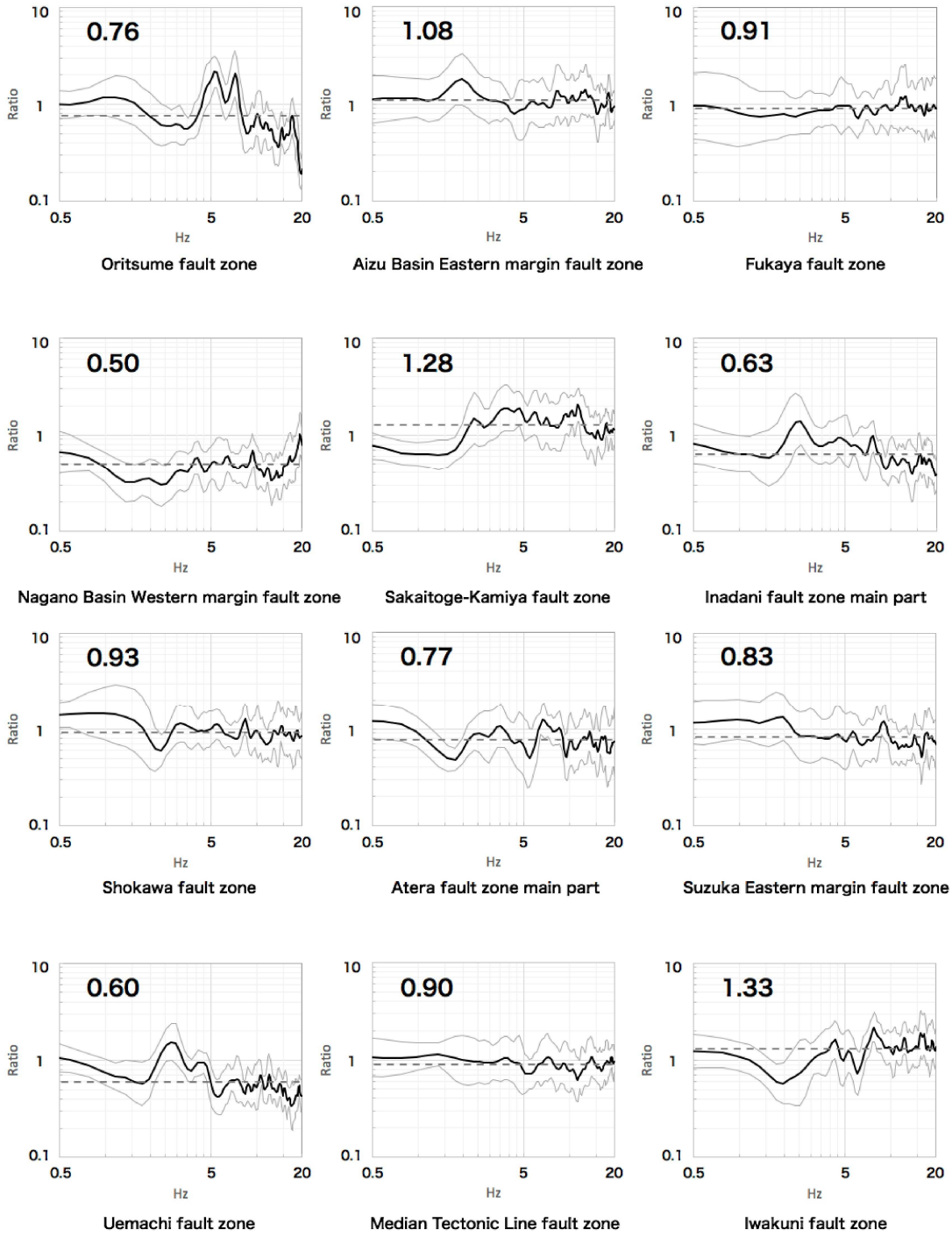

Fig. 6 Twofold spectral ratios in each active fault. The solid line indicates the mean value, the thin solid line indicates the mean plus/minus standard deviation, the dotted line indicates the mean value between 0.5 Hz and 20 Hz (mean twofold spectral ratio), and the numerical values in the graphs show the values of the mean twofold spectral ratio.

Table 3 Standard deviation of spectral ratios of active faults

Active fault	East side	West side
Oritsume fault zone	0.19	0.20
Aizu Basin eastern margin fault zone	0.19	0.23
Fukaya fault zone	0.29	0.19
Nagano Basin western margin fault zone	0.23	0.17
Sakaitoge-Kamiya fault zone	0.19	0.21
Inadani fault zone main part	0.21	0.19
Shokawa fault zone	0.21	0.20
Atera fault zone main part	0.25	0.21
Suzuka Eastern margin fault zone	0.18	0.25
Uemachi fault zone	0.17	0.15
Median Tectonic Line fault zone	0.21	0.18
Iwakuni fault zone	0.17	0.22

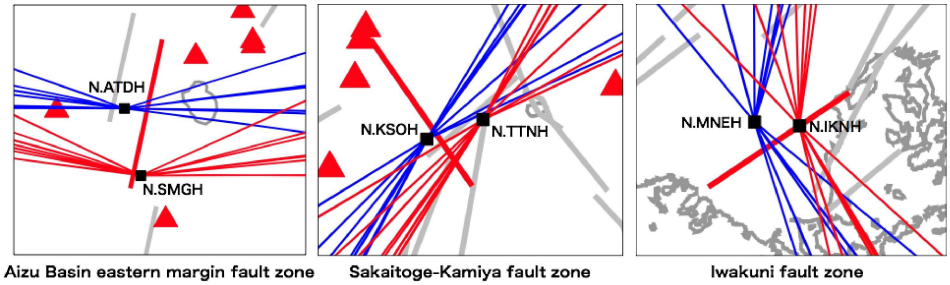

Fig. 7 Spatial location relationship among the observing points (black square), wave line paths (red and blue thin solid line), target active faults (red thick solid line), surrounding active faults (gray solid line) and volcanoes (red triangle)

5.3 Determination of Q values

We determined the Q values from equation (8) for the active faults where the mean twofold spectral ratio is 0.7 or less and a clear attenuation tendency is confirmed. The result is as shown in figure 8. The P-wave velocity in the calculation of Q values is set to 6 km/s. Although a slight unevenness is presented, the Q values for the Oritsume, Nagano Basin western margin, Inadani, and Uemachi fault zones are nearly the same. The Q values for the Atera fault zone and the Suzuka eastern margin fault zone are slightly larger than those values. It can be said that any of these Q values are smaller and the attenuation is larger than those in general crust. As the following equations are used in seismic-wave simulations: $Q_p = Q_s$ and $Q_p = 2 \times Q_s$, figure 8 includes $130f^{0.77}$ [22] and $100f^{0.7}$ [23] and the twofold lines as the general values. The attenuation characteristics obtained were relatively close to the value of Qp = 100 ~ 256 estimated by Ohtake [24] for the focal region of the 1984 Western Nagano Prefecture Earthquake ($Q_p^{-1} = 3.9 \times 10^{-3} - 10.0 \times 10^{-3}$ in the study).

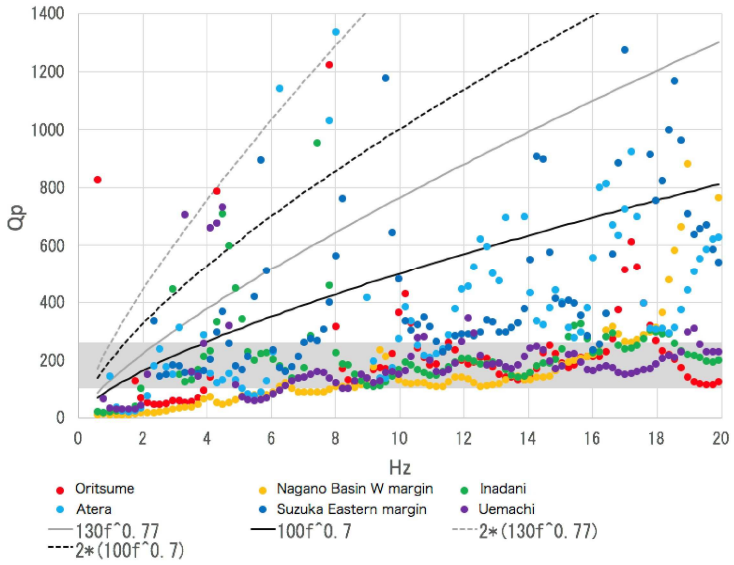

Fig. 8 Q_p values estimated using the twofold spectral ratio method
The gray shaded parts indicate the range of Q_p = 100–256.

5.4 Cases where the observation points do not cross an active fault

To examine whether the mean twofold spectral ratio obtained in this study is attributable to active faults, we conducted an analysis with observation point pairs that do not cross an active fault. As the location is in the vicinity of pairs crossing active faults as previously described and has few active volcanoes, we selected the following two points: in the vicinity of the Oritsume fault zone and in the vicinity of the Median Tectonic Line fault zone. The locational relationship of the observation points and the active faults was used, and the obtained twofold spectral ratios are as shown in figure 9. According to the results of analysis, the mean twofold spectral ratio is 1.01 in the vicinity of the Oritsume fault zone and 0.97 in the vicinity of Median Tectonic Line fault zone. These are larger values than those of the cases with observation points crossing an active fault (0.76 and 0.90, respectively) at both locations. It is suggested that the inhomogeneity in the crust between the observation points is low and the attenuation is small in the cases with the observation points not crossing an active fault. For the cases with observation points crossing an active fault that present a significant reduction in the twofold spectral ratio, it can be said that it is highly likely that the mean twofold spectral ratio obtained from the pairs of observation points crossing the active fault reflects the attenuation characteristics of the active fault.

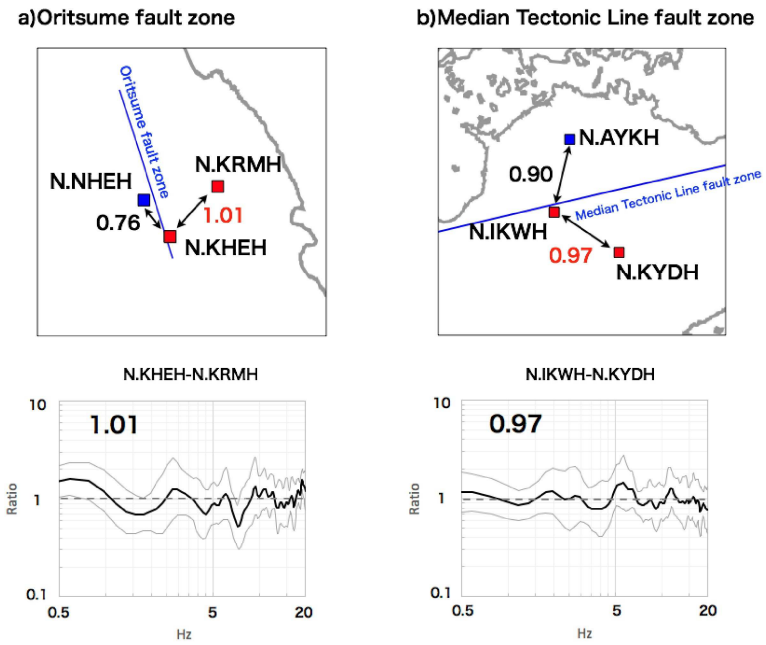

Fig. 9 Twofold spectral ratio in the cases where the observing points do not cross the active fault: (a) Oritsume fault zone (b) Median Tectonic Line fault zone. The red square in the figure indicates the observing point pair not crossing the active fault. The blue square indicates an observing point used for the analysis with the observing point crossing the active fault.

5.5 Relation to the width of fault fracture zones

It has been confirmed that the attenuation characteristics differ depending on the active fault. First, we examined the difference in the width of fault fracture zones that can affect attenuation. Ogata [25] presented the relationship between the fault fracture zone width and the fault length in equation (9) as follows:

$$\log L = 0.68 + 0.87 \log W \tag{9}$$

In this equation, L indicates the length (m) of the fault and W is the width (cm) of the fault fracture zone. By determining the fracture zone width of each active fault using equation (9), we surveyed the relation to the mean twofold spectral ratio (Figure 10). As discussed in Section 5.2, we did not cover a mean twofold spectral ratio exceeding 1 in the discussion because it is possible that it does not express the characteristics of the active faults. In the correlation of the mean twofold spectral ratio and the fault fracture zone width, the correlation coefficient is R = 0.37; thus, a slight positive correlation is observed. However, it can be said that the influence of fault scale on the attenuation characteristics is small in the frequency ranges covered in this study.

Also, a reduction in spectral ratio with a large contour is seen between 0.8 Hz and 4 Hz in the Oritsume fault zone, whose cause may be related to inhomogeneity in some factors. When assuming that the mean P-wave velocity is 5.5 km/s in consideration of the ray paths according to Table 2 and that the P-wave velocity is reduced to approximately 50% in the fracture zone, the wave length corresponding to that between 0.8 Hz and 4 Hz is between 0.7 km and 3.4 km. On the other hand, as the fault fracture zone width of the Oritsume fault zone calculated using equation (9) is approximately 0.4 km, when taking into consideration the first-order vibration is fixed at both ends, it may be corresponding to the wave length previously described. However, in this study, we decided to focus on the mean rate of reduction in spectral ratio without referring to the characteristics for each frequency because of the restrictions on the observation points, seismic data, and other appropriate items.

5.6 Relation to the time-lapse rate

In this section, we examine the possibility of the reflection of the stress state. We conducted a comparison to the time-lapse rate in the long-term evaluation by the Earthquake Headquarters as the parameters that reflect stress state. The time-lapse rate released by the Earthquake Headquarters is a value calculated by dividing the lapse time from the latest activity period to the evaluation time by the mean activity interval. Accordingly, the greater the time-lapse rate is, the further the stress accumulation may increase. In the case that the time-lapse rate has time width, we used the mean value. Figure 11 shows the relationship between the mean twofold spectral ratio value and the time-lapse rate. According to the figure, a positive correlation between the twofold spectral ratio and the time-lapse rate is confirmed, except for the Uemachi fault zone. As for the most recent event period of the Uemachi fault zone, Sugito and Kondo [26] noted a possibility that it may be later than that in the evaluation by the Earthquake Headquarters. When examining the correlation between the mean twofold spectral ratio and the time-lapse rate excluding the Uemachi fault zone based on this, the correlation coefficient is: R = 0.70, presenting a clear positive correlation. These results suggest, interestingly, that the extent of attenuation can reflect the stress accumulation process.

Several studies discuss the attenuation characteristics in faults and the variations [4), 5), 6), 7), 24)]. For example, Chun et al. [5] noted that cracks and the degree of saturation by a fluid in the focal region are the main factors of the changes in the attenuation characteristics. However, many of the studies discuss short-term variations before and after the occurrence of an earthquake, rather than from a long-term point of view. On the other hand, this study has estimated the attenuation characteristics of a number of active faults possibly at different stages in the stress accumulation process, and accordingly, it can be said that this study has discussed changes in attenuation characteristics from a long-term point of view compared to that of existing studies.

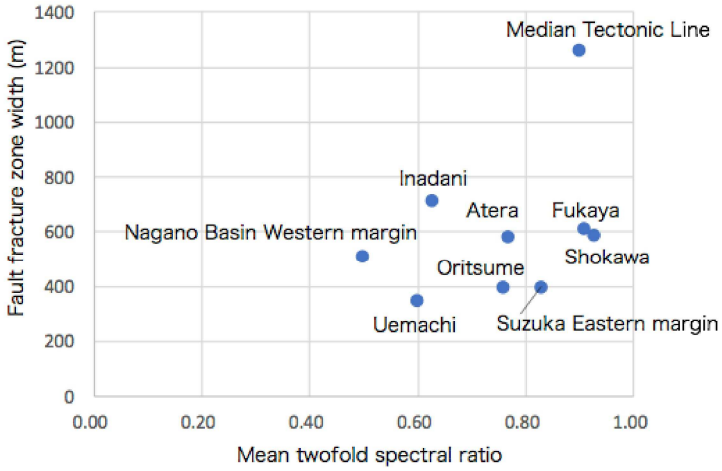

Fig. 10 Relationship between the mean twofold spectral ratio and fault fracture zone width

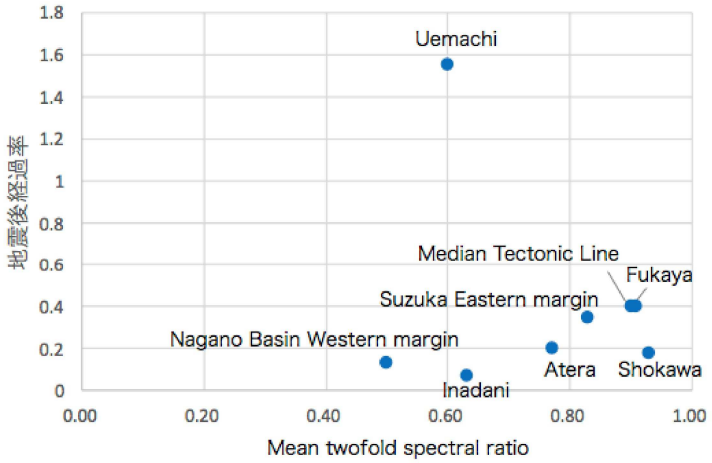

Fig. 11 Relationship between the mean twofold spectral ratio and time lapse rate

6. CONCLUSIONS

In this study, we have estimated the attenuation characteristics of 12 major active faults by applying the twofold spectral ratio method to P-wave first motions.

In the analysis, we selected the pairs of observation points crossing the active fault, and a total of 14 earthquakes, or seven earthquakes from both sides of the active fault among the earthquakes that are at a distance of five times (or greater) away as the observation point interval. Furthermore, we confirmed that the earthquakes passed through the active fault according to the ray tracing. As a result, we successfully estimated the attenuation characteristics after eliminating the source and propagation path characteristics to the vicinity of fault, and the site-amplification characteristics.

As a result of the analysis, it became clear that the attenuation characteristics differ depending on each active fault. And it was also confirmed by the determination of Q value that the Q value of an active fault with a large attenuation is smaller than that of the general crust. According to the results of the examination in the difference in attenuation characteristics, a clear correlation with fracture zone scale was not seen. On the other hand, it was clarified that there is a positive correlation with time-lapse rate. These results suggest that the attenuation characteristics extracted using the twofold spectral ratio method can reflect the stress state of an active fault, i.e., the urgency of the occurrence of an earthquake.

ACKNOWLEDGMENT

In developing this study, we used the Hi-net data from the NIED. We also sought cooperation from Mr. Daiki Hirashima, a Graduate School student (at the time) at Tokyo Metropolitan University, for the organization and analysis of data. We would like to express our gratitude to both.

APPENDIX A: Ray path (Figure 4)

The overview (left figure) and the enlarged view (right figure) are provided for each active fault. The red solid line in the figure indicates the target active fault. Note that the notations of the observing point reflect the depth of high-net stations.

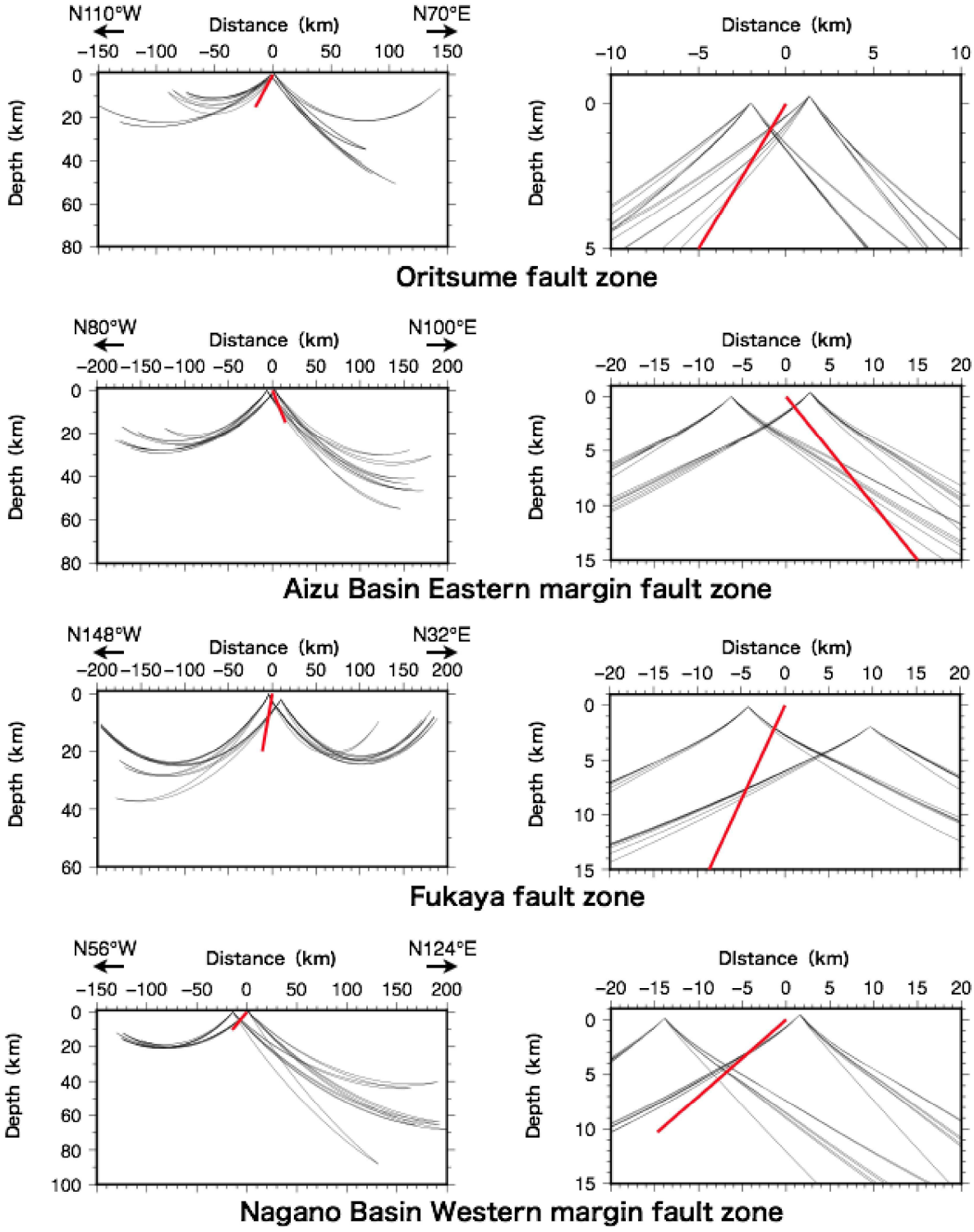

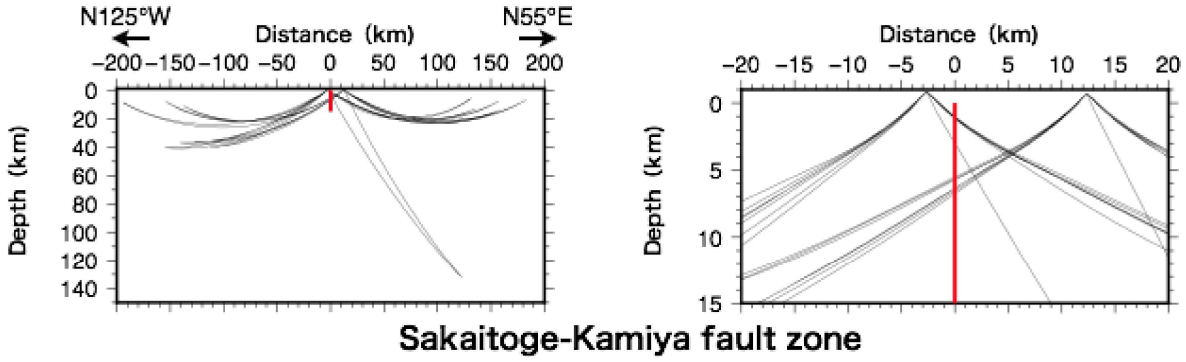

Sakaitoge-Kamiya fault zone

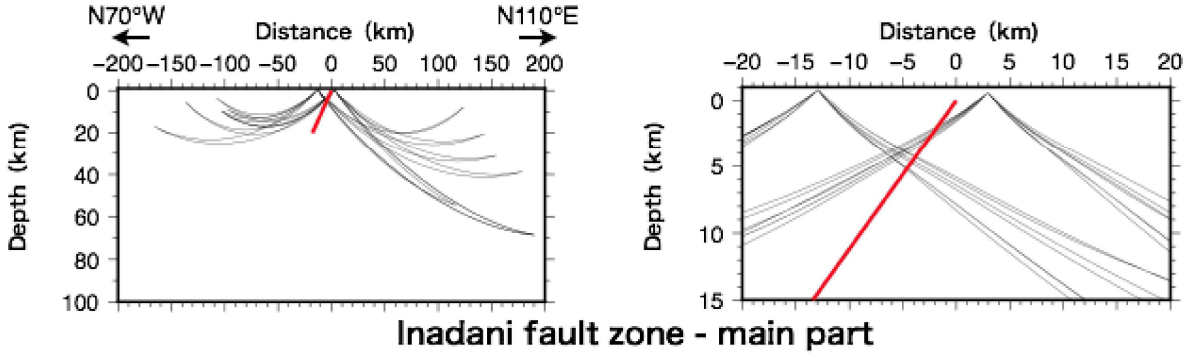

Inadani fault zone - main part

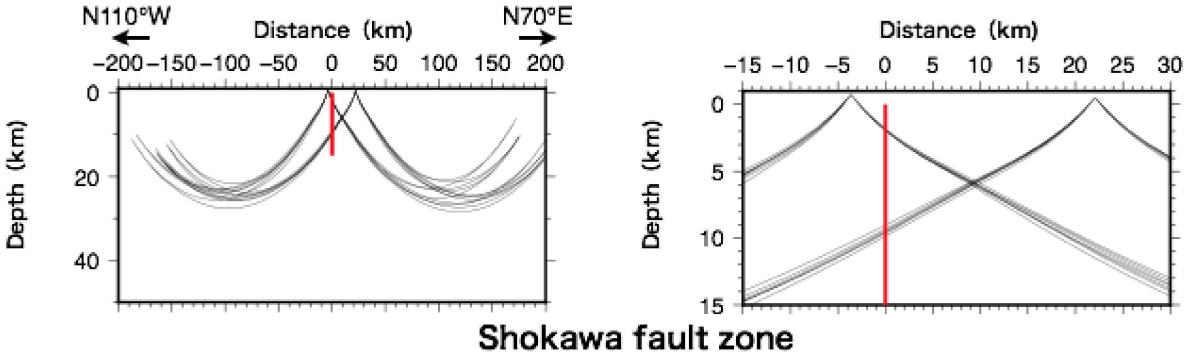

Shokawa fault zone

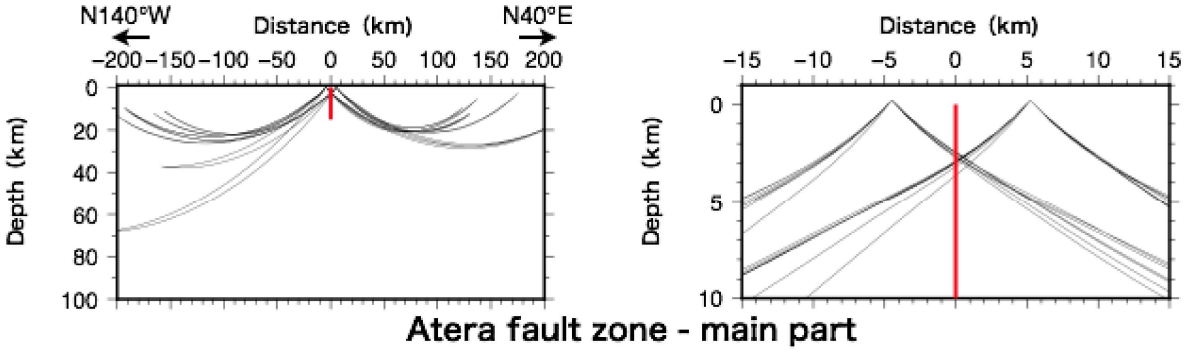

Atera fault zone - main part

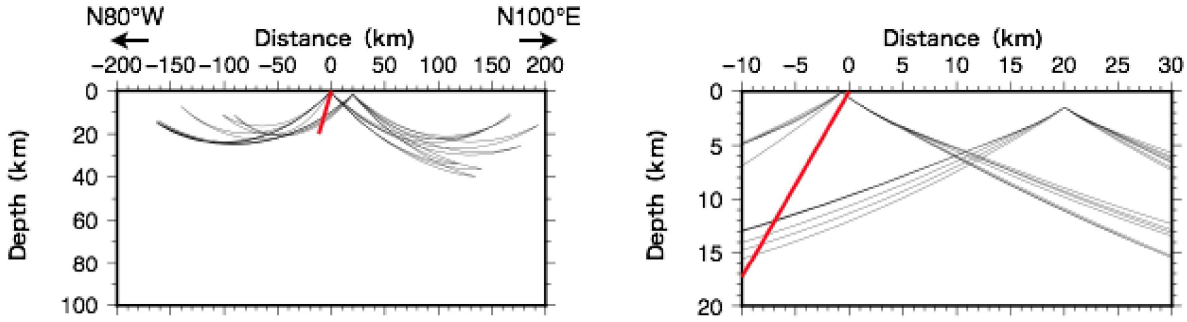

Suzuka Eastern margin fault zone

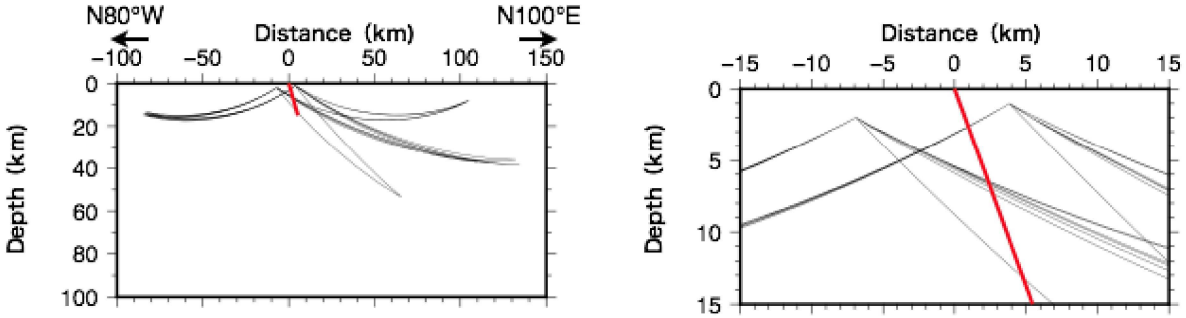

Uemachi fault zone

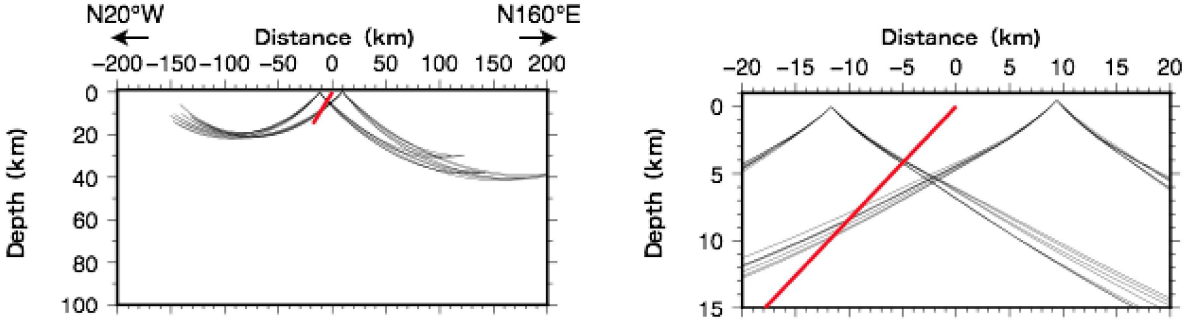

Median Tectonic Line fault zone

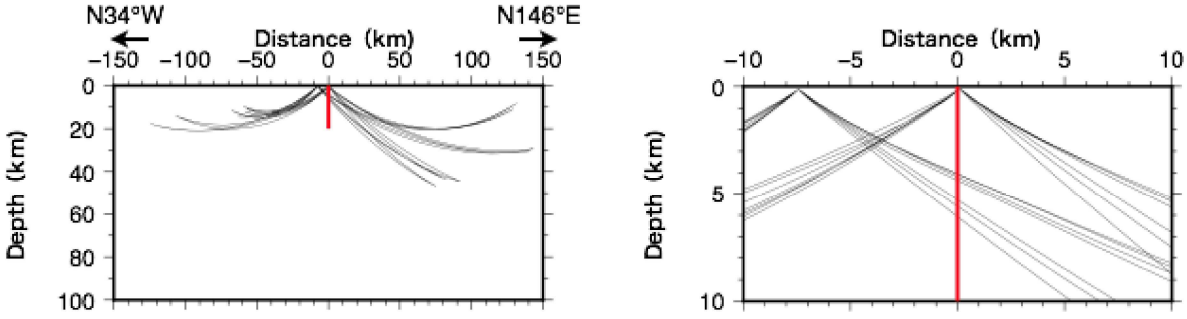

Iwakuni fault zone

APPENDIX B: Spectral ratios from both the directions (Figure 5)
The spectral ratio of the earthquakes on the east side (left figure) and the spectral ratio of the earthquakes on the west side (right figure) are shown.

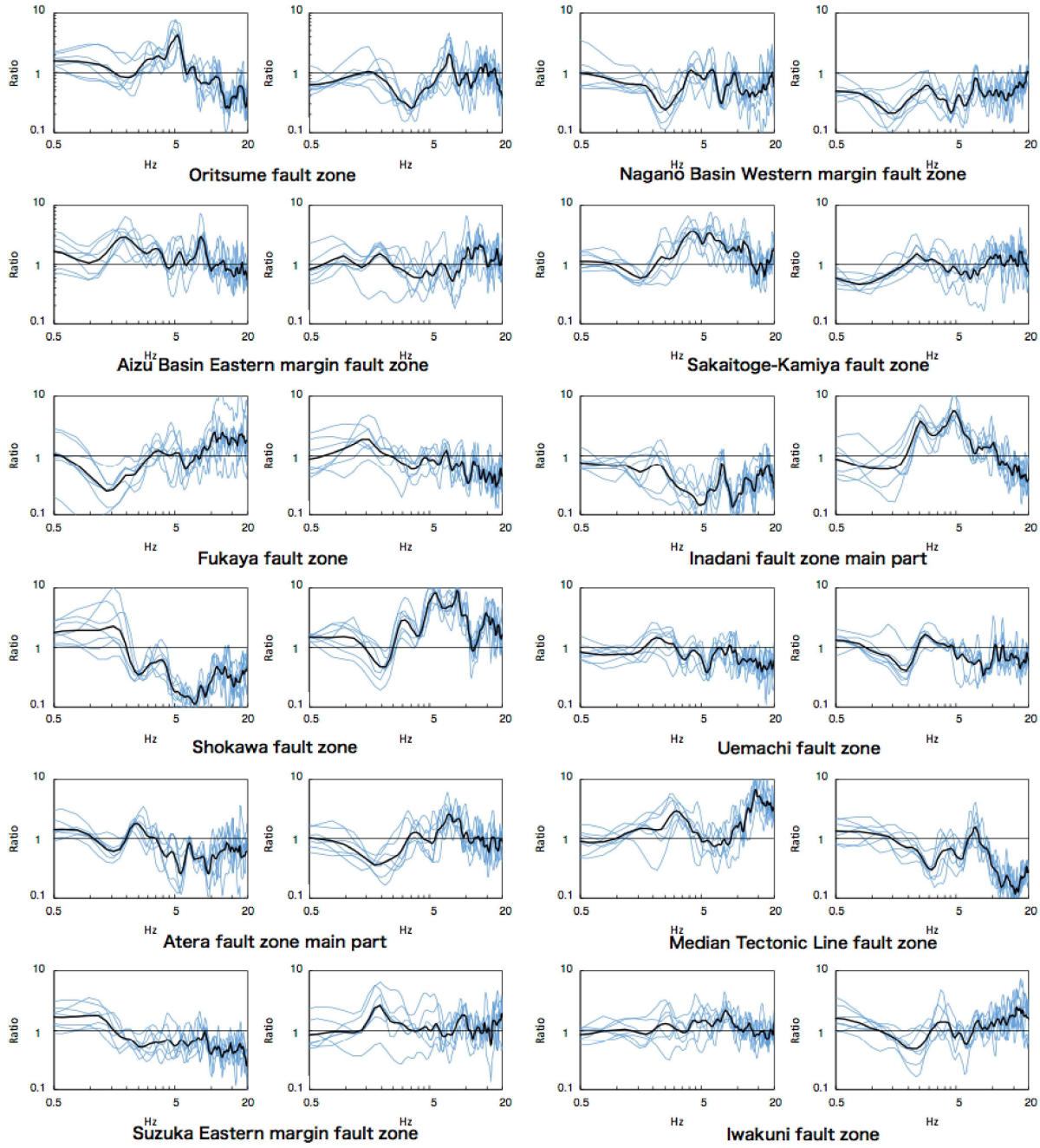

REFERENCES

1) Poupinet, G., Ellsworth, W. L. and Frechet, J.: Monitoring Velocity Variations in the Crust using Earthquake Doublets: An Application to the Calaveras Fault, California, *J. Geophys. Res.*, Vol. 89, pp. 5719-5731, 1984.
2) Uchida, N., Nishimura, T., Yoshimoto, K., Nakahara, H, Sato, H., Ohtake, M., Tanaka, S. and Hamaguchi, H.: Temporal Change of Seismic-wave Velocity Associated with the 1998 Northern

Iwate Prefecture, Japan Earthquake, *Zisin 2, Journal of the Seismological Society of Japan*. 2nd series, Vol. 55, pp. 193–206, 2002.
3) Nakamura, S., Kubo, A., Ohkura, T. and Ouchi, T.: Attenuation of Seismic Waves along the Rokko Fault Zone, *Zisin 2*, Vol. 50, pp. 173–182, 1997.
4) Lees, J. M., Lindley, G. T.: Three-dimensional Attenuation Tomography at Loma Prieta: Inversion of t* for Q, *J. Geophs. Res.*, Vol. 99, pp. 6843-6863, 1994.
5) Chun, K.-Y., Henderson, G. A. and Liu, J.: Temporal Changes in P wave Attenuation in the Loma Prieta Rupture Zone, *J. Geophys. Res.*, Vol. 109, B02317, doi:10.1029/2003JB002498, 2004.
6) Blakeslee, S., Malin, P. and Alvarez, M.: Fault-zone Attenuation of High-frequency Seismic Waves, *Geophys. Res. Lett.*, Vol. 16, pp. 1321-1324, 1989.
7) Yamada, M., Idota, Y., Oda, Y. and Ito Y.: Temporal change in spectrum ratio related to the Iwate-Miyagi Nairiku Earthquake in 2008, *The 14th Japan Earthquake Engineering Symposium*, pp. 1799–1808, 2014.
8) Matsuzawa, T., Hasegawa, A. and Takagi, A.: Qp Structure beneath the Northeastern Japan Arc Estimated from Twofold Spectral Ratio Method, *Tohoku Geophys. J*, Vol. 32, pp. 21-33, 1989.
9) Yamanaka, Y. and Kikuchi, M.: Q_s^{-1} Value Beneath Mt. Iwate by Means of Twofold Spectral Ratio Method, *Zisin 2*, Vol. 51, pp. 457–458, 1999.
10) Izutani, Y.: Qs-value in Southern Kyushu Evaluated from Double Spectral Ratio of Strong Motion Records, *Journal of the Japan Society of Civil Engineers*, No. 640/I-50, pp. 225–230, 2000.
11) Matsuzawa T., Takeo, M., Ide, S., Iio, Y., Ito, H., Imanishi, K. and Horiuchi, S.: Estimation of the S-Wave Attenuation in the Western Nagano Region from Twofold Spectral Ratio, *Zisin 2*, Vol. 56, pp. 75–88, 2003.
12) Iwata, T., and Irikura, K.: Separation of Source, Propagation and Site Effects from observed S-Waves, *Zisin 2*, Vol. 39, pp. 579–593, 1986.
13) Watanabe, T. and Sassa, K.: Attenuation Tomography by Use of First Peak Amplitude of Seismic Wave, *Geophysical Exploration*, Vol. 45, pp. 10–21, 1992.
14) The Headquarters for Earthquake Research Promotion: Long-Term Evaluations of Active Faults.http://www.jishin.go.jp/evaluation/long_term_evaluation/major_active_fault/ (accessed on July 15, 2017)
15) Borcherdt, R. D.: Empirical Evidence for Acceleration-dependent Amplification Factors, *Bull. Seism. Soc. Am.*, 92, pp. 761-782, 2002.
16) Fujimoto, K. and Midorikawa, S.: Relationship between Average Shear-Wave Velocity and Site Amplification Inferred from Strong Motion Records at Nearby Station Pairs, *Journal of Japan Association for Earthquake Engineering*, 6, pp. 11–22, 2006.
17) Um, J. and Thurber, C: A Fast Algorithm for Two-point Seismic Ray Tracing, *Bull. Seismol. Soc. Am.*, Vol. 77, pp. 972-986, 1987.
18) Ueno, H., Hatakeyama, S., Aketagawa, T., Funasaki, J. and Hamada, N.: Improvement of hypocenter determination procedures in the Japan Meteorological Agency, *Quarterly Journal of Seismology*, Vol. 65, pp. 123–134, 2002.
19) Evance, J. R., Eberhart-Phillips, D. and Thurber, C. H.: User's Manual for SIMULPS12 for Imaging Vp and Vp/Vs: A Derivative of the "Thurber" Tomographic Inversion Simul3 for Local Earthquakes and Explosions, *USGS-OFR-94-431*, 1994.
20) Japan Seismic Hazard Information Station (J-SHIS) http://www.j-shis.bosai.go.jp/ (accessed on June 17, 2017)
21) Japan Meteorological Agency: National Catalogue of the Active Volcanoes in Japan (The Fourth Edition), 2013.
22) Fukushima, Y.: Survey on Recent Studies on Attenuation Relation of Strong Ground Motion (Empirical Prediction Relation), *Zisin 2*, Vol. 46, pp. 315–328, 1993.
23) Kinoshita, S.: Evaluation of Site Factor and Propagation Characteristics by Means of Earthquake observation, *Zisin 2*, Vol. 46, pp. 161–170, 1993.
24) Ohtake, M.: Temporal change of Q_P^{-1} in Focal Area of 1984 Western Nagano, Japan, Earthquake as Derived from Pulse Width Analysis, *J. Geophys. Rec.*, Vol. 92, pp. 4846-4852, 1987.

25) Ogata, S: Activity Evaluation of Fault in the Basement Terrain-characteristics of its Fracture Thickness and Filled Materials, *Jour. Japan Soc. Eng. Geol.*, Vol. 17, pp. 119-121, 1976.
26) Sugito, N. and Kondo, H.: Most Recent Faulting Event in the Uemachi Fault Zone and Related Changes in the Geomorphic Environment of Kawachi Plain, Southwest Japan, *Journal of Geography*, Vol. 124, pp. 607–631, 2015.

(Accepted: July 25, 2017)
(Decided to publish: December 27, 2017)

(Original Japanese Paper Published: February, 2018)
(English Version Submitted: October 31, 2018)
(English Version Accepted: December 20, 2018)